A Millimeter Wave Dual-Lens Antenna for IoT-Based Smart Parking Radar System

Zhanghua Cai, *Student Member, IEEE*, Yantao Zhou, Yihong Qi, *Senior Member, IEEE*, Weihua Zhuang, *Fellow, IEEE*, and Lei Deng, *Member, IEEE*

***Abstract*—With a rapid increase in the number of vehicles over recent years, urban parking systems have encountered more and more challenges. In this article, a dual-lens millimeter wave (MMW) radar antenna is designed for a smart parking system in the context of the Internet of Things (IoT). A flat dielectric punch lens is used to increase the gain of the transmitting antenna in order to compensate for the penetration loss in MMW. In addition, a dielectric rod lens is used to correct beam direction and maintain a wide beamwidth in order to overcome received energy loss due to scattering of the car chassis. The combined dual-lens antenna can improve the accuracy and stability of MMW radar operating at 24 GHz. The measured gain is 15.8 dBi for the transmitting antenna and 7.9 dBi for the receiving antenna, and the 3-dB beamwidth is approximately 65°. The system measurement results show that the proposed antenna has stable measurement effect and is suitable for the MMW radar smart parking system.**

***Index Terms*—Dielectric rod lens, dual-lens antenna, flat lens, millimeter wave (MMW) radar, smart parking system.**

I. Introduction

With rapid increase of the number of motor vehicles, along with limited parking spaces, has led to a series of parking-related problems [1], [2]. Drivers must often spend long periods searching for parking spaces, causing issues such as fuel waste, air pollution, and traffic jams.

Smart parking systems and the Internet-of-Things (IoT) technologies have a great potential to alleviate this phenomenon [3], [4]. Intelligent parking systems can usually obtain information about available parking spaces in a specific geographic area and process them in real time to facilitate parking and charging. Furthermore, the IoT paradigm will enable things in the environment to connect to the Internet and make it easy to access them from any remote location. The wireless detection nodes used in the smart parking system can be connected to remote devices through IoT technology.

Currently, among the many vehicle detection methods, parking meters, video cameras [5], [6], and magnetic sensors [7]–[9] are the most common. On-street parking lots with parking meters or parking pay stations are expensive. Moreover, parking meters are passive and can be used only for charging; they cannot provide available parking space information to the administrators or drivers. Video cameras are susceptible to weather factors. In addition, camera systems with image processing capabilities are expensive. The cost of densely deploying cameras to monitor each parking space is high. Therefore, they are not good options for economical intelligent parking information systems.

In recent years, magnetic sensors have been widely used in parking systems. For parking space detection, they have many advantages, such as low-power consumption, easy to install, not easily damaged, and low cost. Thus, magnetic sensors provide an ideal, economical solution for smart parking. However, magnetic sensors are susceptible to interference, especially in a complex environment such as an on-street parking lot. Surrounding vehicles and other ferromagnetic objects can distort signals from magnetic sensors, resulting in potential errors. Therefore, the detection accuracy of a single magnetic sensor is low [10], [11].

A millimeter wave (MMW) radar can be integrated with a magnetic sensor. The MMW radar can detect the presence of a car by the echo signal. Considering that the MMW radar has high power consumption while the magnetic sensor has low-power consumption, the high sensitivity of the magnetic sensor can be used to wake up the MMW radar. By combining and comparing the results from the two modules, we can determine whether there is a vehicle in the parking space. Therefore, a dual-mode detection system consisting of a magnetic sensor and an MMW radar can improve the accuracy of parking space detection while maintaining low-power consumption.

The main factor affecting the accuracy of a radar detection system is the performance of its antenna. A dual-mode detection technology combining geomagnetic sensor and Doppler radar is proposed in [12]. The whole system is described in [12] but the performance of the MMW radar and antenna design requirements are not analyzed. The MMW antenna should have a sufficiently high transmitting energy and be able to receive a sufficiently

Manuscript received February 6, 2020; revised May 29, 2020; accepted June 19, 2020. Date of publication June 23, 2020; date of current version December 21, 2020. This work was supported by the National Natural Science Foundation of China under Grant 61671203. *(Corresponding authors: Zhanghua Cai; Yantao Zhou.)*

Zhanghua Cai and Yantao Zhou are with the School of Electrical and Information Engineering, Hunan University, Changsha 410082, China (e-mail: zhanghua.cai@generaltest.com; yantao_z@hnu.edu.cn).

Yihong Qi is with Peng Cheng Laboratory, Shenzhen 518000, China, also with the Research and Development Department, Linke, Zhuhai 519000, China, also with the School of Electrical and Information Engineering, Hunan University, Changsha 410082, China, also with the EMC Laboratory, Missouri University of Science and Technology, Rolla, MO 65409 USA, and also with Western University, London, ON N6A 3K7, Canada (e-mail: qiyh@pcl.ac.cn).

Weihua Zhuang is with the Department of Electrical and Computer Engineering, University of Waterloo, Waterloo, ON N2L 3G1, Canada (e-mail: wzhuang@uwaterloo.ca).

Lei Deng is with the Department of Electronics and Information Engineering, Hunan University, Changsha 410082, China (e-mail: lei.deng@linketech.cn).

Digital Object Identifier 10.1109/JIOT.2020.3004403

2327-4662 © 2020 IEEE. Personal use is permitted, but republication/redistribution requires IEEE permission.
See https://www.ieee.org/publications/rights/index.html for more information.

Authorized licensed use limited to: HUNAN UNIVERSITY. Downloaded on March 04,2021 at 08:46:03 UTC from IEEE Xplore. Restrictions apply.

large portion of the reflected energy. A linear frequency modulation continuous wave (LFMCW) radar is considered for this application. Due to the need to continuously transmit signals, the transmitting and receiving antennas should use two independent antennas. Furthermore, because of the space limitation, the distance between the transmitting and receiving antennas should be small.

Due to large MMW penetration loss, the transmitting antennas should have a high gain in order to make the MMW radar achieve proper penetration effect, thus enhancing the accuracy and reliability of detection. On the other hand, we cannot blindly pursue a high gain for the receiving antenna. Note that the car chassis structure is complex, not an ideal plane. Scattering occurs from reflectors, such as wedge and cylindrical surfaces. In this case, the reflected wave received by the receiving antenna may come from different directions, and the high energy may not be received in the main direction of the antenna. Therefore, the antenna is required to have a relatively wide beamwidth, without gain zero points in the possible reception range. High gain antennas usually have gain zeros in a very narrow beam range. If the reflected wave falls within the zero range of the receiving antenna, the received energy will be too small, and misjudgment can occur.

The dielectric lens is widely used in the MMW band to improve antenna gain [13]–[16]. Compared with the traditional method of increasing gain through arrays (such as patch antenna array [17], slot antenna array [18], and dipole antenna array [19]), lens antennas have the advantages of low cost and low loss. They can avoid the use of large-area expensive MMW substrate, complex and expensive processing technology, and do not need to design a complex feed network. The lens can be used for this parking radar system to increase the transmitting antenna gain. However, the dielectric lens has a relatively large size. When the transmitting and receiving antennas are very close, the lens will affect the radiation pattern of the receiving antenna, causing its beam to shift. Therefore, a new solution is required to correct the beam direction of the receiving antenna and achieve a wide beamwidth.

There are various ways to change antenna beamwidth. One is to change the structure of the radiation unit [20], [21]. Another way is to exploit the deformation of the reflector [22], [23]. The third commonly used method is by loading the parasitic structure [24], [25]. While all the methods can change the beamwidth, it is relatively difficult to correct the beam offset caused by the transmitting antenna lens. In general, the antenna pattern is designed symmetrically, which makes it difficult to change the beam direction by adjusting a single unit. In addition, the antenna size for the MMW band is small. The small metal reflector and parasitic structures are not easy to manufacture and the error can be large. The structural complexity of the system also increases.

A transmitting and receiving dual-lens radar antenna is proposed in this article. On the one hand, the gain of the transmitting antenna is improved by using a flat perforation lens. On the other hand, the function of the dielectric to guide the electromagnetic wave is used to design a cone-shaped dielectric rod lens to correct the beam of the receiving antenna [26]. At the same time, the receiving antenna maintains a wide beamwidth, and there is no obvious gain zero in a wide angle. The method of using a lens to correct the beam has a high design tolerance, avoiding complicated unit design and manufacturing of small metal structural parts. The combined dual-lens antenna not only makes the radar have sufficient penetrating ability but also ensures that the radar can receive sufficient energy in a wide angle, which improves the accuracy and reliability of the system detection.

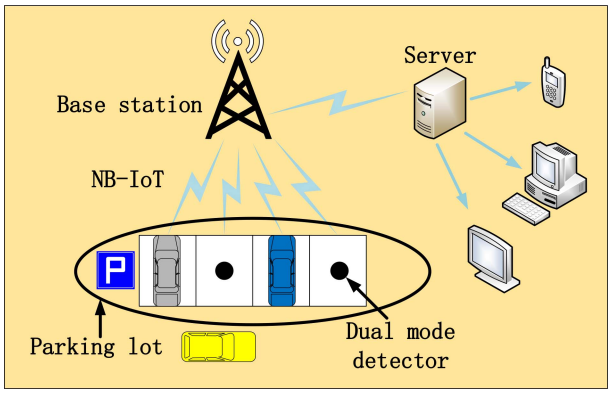

Fig. 1. Illustration of the smart parking system.

The remainder of this article is structured as follows. Section II introduces the IoT-based smart parking system. Section III describes the design of the dual-lens antenna. Section IV discusses the measured results of the antenna and the system, followed by conclusions of this work in Section V.

II. System Model

A. Overview of the Smart Parking System

Fig. 1 shows the overall system framework of an intelligent parking system under consideration. The system consists of a dual-mode detector, a background server, and a user device. The dual-mode detector primarily consists of a geomagnetic sensor, an MMW radar, and a narrowband IoT (NB-IoT) wireless module. The parking space detector determines the current parking space status and transmits real-time parking space information to the server through the NB-IoT. The background server can provide this parking space information to a smart phone terminal, parking guide screen, or PC client for users to query.

The use of NB-IoT technology for wireless communication has numerous advantages [27]–[29]: 1) NB-IoT has a long communication distance and wide coverage, and can directly use the operator network without the need for relay installation; 2) NB-IoT uses a licensed spectrum, resulting in less interference and more stable and reliable in comparison with other methods using unlicensed spectrum; 3) NB-IoT has low-power consumption, without a need to replace device batteries for several years; and 4) the narrow bandwidth and low-power consumption of NB-IoT correspond to low radio-frequency (RF) design requirements, which brings the advantage of low cost to the module.

Authorized licensed use limited to: HUNAN UNIVERSITY. Downloaded on March 04,2021 at 08:46:03 UTC from IEEE Xplore. Restrictions apply.

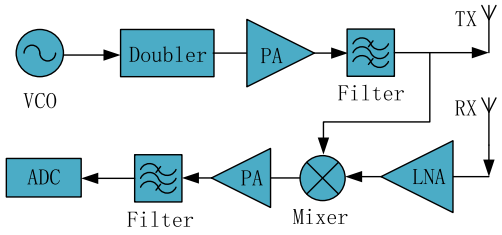

Fig. 2. Block diagram of the RF front-end architecture.

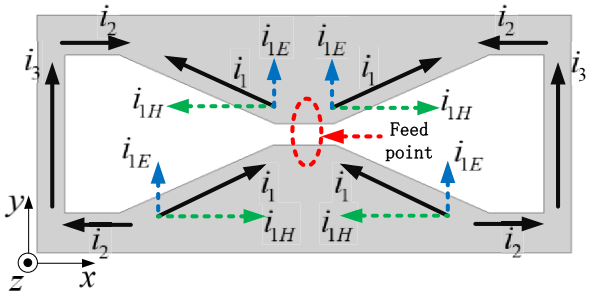

Fig. 3. Original structure and current distribution of the WHEMS antenna.

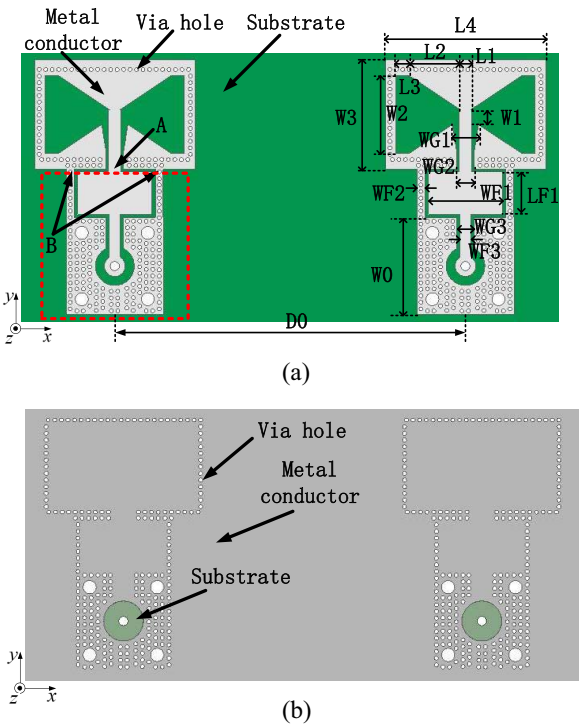

Fig. 4. Structure of the proposed primary antenna. (a) Top view. (b) Bottom view.

TABLE I
GEOMETRIC PARAMETERS OF THE PROPOSED ANTENNA (UNIT: MM)

Parameter	Value	Parameter	Value	Parameter	Value
L1	1.0	W0	7.5	WF2	0.6
L2	3.8	W1	1.0	WF3	0.8
L3	1.0	W2	6.0	WG1	2.0
L4	12.3	W3	8.4	WG2	1.3
LF1	3.7	WF1	5.7	WG3	1.3

B. MMW Radar System Framework

A block diagram of the RF front-end architecture of the LFMCW device is shown in Fig. 2. Frequency-modulated (FM) triangular continuous signals are generated at a 12-GHz voltage-controlled oscillator (VCO) and are doubled to obtain a 24-GHz signal. The FM signal is transmitted via the transmitting antenna after being amplified and filtered. The electromagnetic waves are reflected when they encounter metal objects such as the car chassis, and the echo signal is received by the receiving antenna. A mixed-frequency signal is obtained by mixing the transmitted signal with the received signal. This mixed-frequency signal provides information, such as distance and energy, which can be used to detect if there is a vehicle in a parking space.

III. LENS ANTENNA DESIGN

A. Primary Antenna Design

The design of the primary feed antenna is based on a wideband high-efficiency structure (WHEMS) (also known as a slot loop antenna) [30]–[35]. The initial structure of the WHEMS antenna is shown in Fig. 3, where the filled area is composed of a metal conductor. The basic WHEMS consists of two symmetrical polygonal slots, and the feed point is located in the center gap (as shown in Fig. 3). The typical current distribution is shown by the solid line with an arrow, and the dotted line indicates the current decomposed by the oblique current i_1. It can be seen that the currents cancel each other in the horizontal direction and that multiple currents are superimposed in the vertical direction. Therefore, the antenna has a uniform aperture distribution in the H-plane.

Fig. 4 depicts the WHEMS MMW antenna model used in this work. The antenna is etched on a 1-mm-thick F4b substrate, and the relative dielectric constant is 2.2. The center distance between the receiving and transmitting antennas D0 is 27 mm (according to the requirements for an actual product). The component in the red dashed box is the SMP connector position reserved for passive testing, which does not exist in the actual system. In the actual system, position A is connected to the signal line and position B is grounded. This feeding method does not require an additional connector, conveniently integrating the antenna with the RF circuit. It should be noted that because the port in the actual system is different from the SMP port shown in Fig. 4, the antenna parameters in Fig. 4 are only used for passive testing to verify the correctness of the design. When the antenna is used in the system, the parameters should be adjusted according to the system port connection mode to achieve impedance matching.

In addition, densely grounded vias are added around the current path, making the antenna form a cavity structure. The field on the antenna is confined to the cavity to reduce the loss in the MMW band. The specific dimensions of the antenna are given in Table I.

B. High Gain Flat Lens Design

Briefly, the gain is increased by applying a lens to convert the field in the main radiation direction of the antenna from

Authorized licensed use limited to: HUNAN UNIVERSITY. Downloaded on March 04,2021 at 08:46:03 UTC from IEEE Xplore. Restrictions apply.

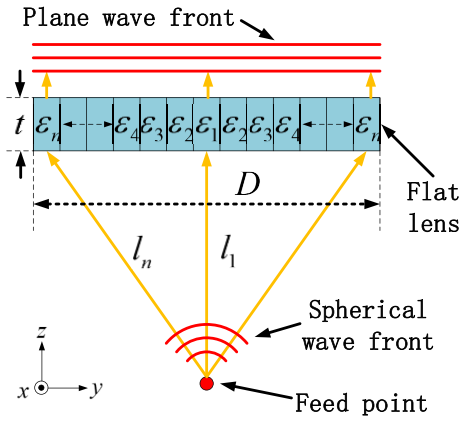

Fig. 5. Functional principle of the dielectric flat lens antenna.

a spherical wavefront to a planar wavefront. In this manner, the electric field forms an in-phase superposition in the main radiation direction, resulting in an increased gain. The function of a lens is to perform phase correction.

Compared with a curved lens antenna, a flat lens can be more easily conformed to the housing of vehicle detector. The working principle of the flat lens is illustrated in Fig. 5. The relative dielectric constant of the flat lens varies with the distance from the center. Therefore, different phase delays will occur for various positions along the flat lens. By adjusting the relative dielectric constant, a plane wave can be formed for an electromagnetic wave passing through the lens. The phase difference between any path, l_n, and path l_1 through the center of the lens is given by

$$\varphi = 2\pi \frac{l_n - l_1}{\lambda_0} \tag{1}$$

where φ is the required corrected phase and λ_0 is the free-space wavelength at the operating frequency. The calibration phase of the lens can be calculated by

$$\varphi = 2\pi \left(\frac{t}{\lambda_1} - \frac{t}{\lambda_n} \right) \tag{2}$$

where t is the thickness of the flat lens as shown in Fig. 5, and λ_1 and λ_n represent the wavelength in a dielectric with permittivity ε_1 and ε_n at the corresponding positions in Fig. 5, respectively. Let us consider the following relationship:

$$\frac{\lambda_0}{\lambda_n} = \frac{v_0/f}{v_n/f} = \sqrt{\mu_{rn}\varepsilon_{rn}} = \sqrt{\varepsilon_{rn}} \tag{3}$$

where v_0 is the free-space speed, v_n is the speed in the dielectric, f is the frequency, ε_{rn} is the relative permittivity of the dielectric, and μ_{rn} is the relative magnetic permeability of the dielectric, which is close to 1 for a nonmagnetic material. Then, λ_1 and λ_n can be replaced, respectively, by $\lambda_0/\sqrt{\varepsilon_{r1}}$ and $\lambda_0/\sqrt{\varepsilon_{rn}}$, and (2) can be modified as

$$\varphi = 2\pi t \frac{\sqrt{\varepsilon_{r1}} - \sqrt{\varepsilon_{rn}}}{\lambda_0}. \tag{4}$$

Producing a substrate from a variety of materials is relatively complicated. Thus, the equivalent dielectric constant is usually achieved by perforation. Fig. 6 presents a top view

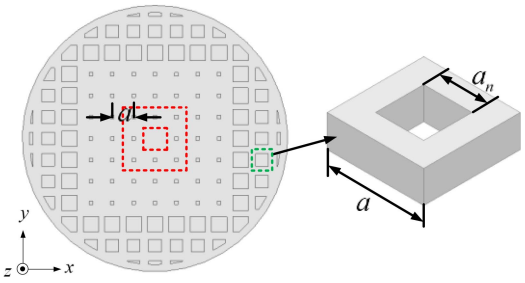

Fig. 6. Model of a flat dielectric perforated lens.

TABLE II
SIDE LENGTH a_n OF EACH LAYER n

n	Calculated a_n (mm)	Optimized a_n (mm)
1	0	0
2	0.61	0.5
3	1.18	0.5
4	1.71	0.5
5	2.18	2.16
6	2.58	1.78

of the flat perforated antenna designed in this work. The lens is composed of acrylonitrile butadiene styrene (ABS), with a relative dielectric constant of approximately 2.7. Due to the requirements of the application, the overall height of the antenna is limited. In addition, because the receiving antenna should not be blocked, the diameter of the lens is also limited. Considering the performance under these limitations, the related parameters were finally determined as $l_1 = 15$ mm, $t = 14$ mm, and $D = 37$ mm.

A magnified model of the perforated unit is shown in Fig. 6, where the square unit has a side length of $a = 3$ mm. The red dotted square ring area represents the same layer, and the square holes in the same layer are designed to be the same size. The distance of each layer from the lens center is approximated by $(n-1)a$ (where $n = 1$ at the lens center). Because the actual antenna is not an ideal point source. The actual source will not be concentrated on a point of the antenna, and the phase centers of different radiation planes are inconsistent. Thus, both rectangular and circular arrangements are approximate analysis methods. In this article, the rectangular arrangement design mainly considers the convenience of modeling and optimization. The equivalent relative dielectric constant of the cell can be approximately calculated by

$$\varepsilon_{rn} = \frac{a_n^2}{a^2}\varepsilon_{r0} + \frac{a^2 - a_n^2}{a^2}\varepsilon_{r1}. \tag{5}$$

Based on (1), (4), and (5), the side length of the square hole for each layer can be calculated. The calculated results can then be set as the initial design value. Several equivalent and approximate methods have been used in the calculation. Since the actual primary antenna is not an ideal point source and has certain aperture, the parameters must be optimized based on an initial value to obtain a maximal gain improvement. The final dimensions are listed in Table II. Since the layer 6 is located at the edge of the lens, an average permittivity of this area should take into account the influence of air.

Authorized licensed use limited to: HUNAN UNIVERSITY. Downloaded on March 04,2021 at 08:46:03 UTC from IEEE Xplore. Restrictions apply.

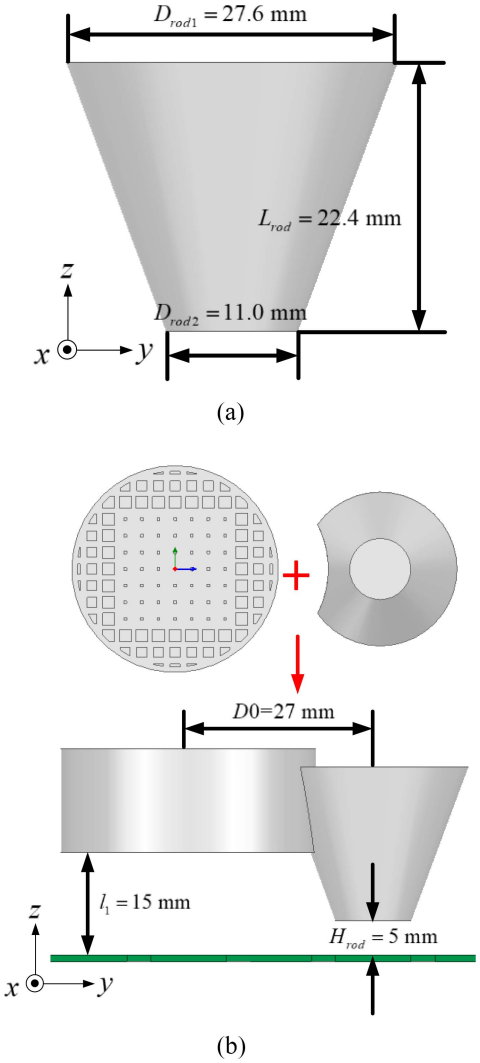

Fig. 7. Model of the (a) dielectric rod lens and (b) combined dual-lens antenna.

Therefore, the optimization result of a_6 is much smaller than the theoretical calculation value and less than a_5.

C. Dielectric Rod Lens Design

Dielectric rods have the effect of conducting electromagnetic waves and are often used in MMW antennas. In this work, the conduction ability of a dielectric rod is used to guide the electromagnetic waves of the receiving antenna so that the high-gain flat lens does not affect the main radiation direction. A cone shaped dielectric rod lens [shown in Fig. 7(a)] is designed to correct the beam offset. The combination of a dielectric rod and a high-gain lens is shown in Fig. 7(b). The center distance between the two lenses is 27 mm (corresponding to the distance between the transmitting and receiving antennas). The region in which the two overlapping lenses remain corresponds to the flat lens, and the region belonging to the dielectric rod is cut off. The parameters for the dielectric rod lens are determined from the following principles.

1) *Shape:* The dielectric rod lens uses the frustum of a cone with a small area bottom and a large-area top, which can reduce the escape of energy to the outside from the rod wall during the conduction process and can prevent the radiation pattern from being altered.
2) *Diameters, D_{rod1} and D_{rod2}:* When the diameter of the dielectric rod is small (less than approximately one-quarter wavelength), the guided wave effect of the rod is weak, and only a small fraction of the energy will be confined in the dielectric rod. Therefore, the diameter of the dielectric rod must not be too small.
3) *Lens Length, L_{rod}:* An excessively long dielectric rod lens will cause the antenna to act as an end-fire antenna (increasing the gain and narrowing the beam). Therefore, a dielectric rod guide is needed only in the range susceptible to high-gain lenses in this case.
4) *Height From the Primary Antenna, H_{rod}:* The bottom surface of the lens must be located at an appropriate distance from the primary antenna. If the distance is too short, the *S*-parameter and radiation performance of the primary antenna may be impacted. If the distance is too great, the guidance effect will be lost. According to the simulation results, an appropriate distance is approximately one half of the wavelength.

Following the above principles, the lens was designed within a limited size range. The actual lens parameters are shown in Fig. 7.

D. Performance Comparison

The simulated *H*-plane electric field and the pattern of the radar antenna are shown in Figs. 8 and 9, respectively, for three states. It can be seen that the radiated electric field of the antenna is a spherical wave in the absence of a lens. When only the high-gain flat lens (lens A) is added to the transmitting antenna (left), the electric field in the main radiation direction of the transmitting antenna is transformed to an approximately planar wave, demonstrating that the lens improves the phase alignment and antenna gain. However, the lens also shifts the electric field of the receiving antenna (right). Thus, there is only a small gain in the receiving range, which can affect the measurement results. When the combined dual-lens (lens B) is used, the field of the receiving antenna is guided by the dielectric rod lens to radiate in the main direction, with no offset. The *H*-plane 3-dB beamwidth of the receiving antenna is approximately 60°, and there are no obvious zero-gain points over a wide angle. The field along the main direction of the transmitting antenna is primarily unaffected by the dielectric rod lens. A simulated comparison of the antenna gain with and without the dual-lens is shown in Fig. 10. It demonstrates that the gain of the transmitting antenna at 24 GHz is improved by about 8 dB and the gain of the receiving antenna is improved by about 1 dB while maintaining a wide beamwidth.

IV. Measurement and Analysis

A. Antenna Measurement Results

The proposed dual-lens antenna prototype used for passive testing is shown in Fig. 11. The combined dielectric dual-lens is formed in one step using 3-D printing technology. The lens is fixed on the hole of the substrate by edge pillars, and the

Authorized licensed use limited to: HUNAN UNIVERSITY. Downloaded on March 04,2021 at 08:46:03 UTC from IEEE Xplore. Restrictions apply.

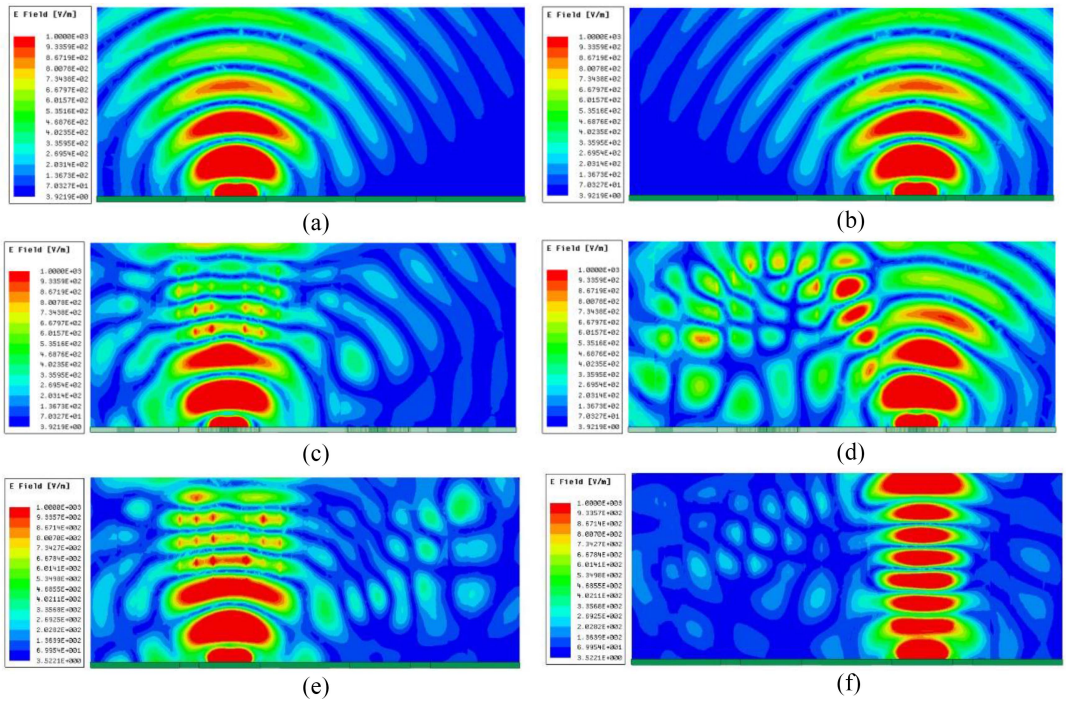

Fig. 8. Electric field distribution of the proposed antenna. (a) H-plane of the transmitting antenna with no lens. (b) H-plane of the receiving antenna with no lens. (c) H-plane of the transmitting antenna with lens A. (d) H-plane of the receiving antenna with lens A. (e) H-plane of the transmitting antenna with lens B. (f) H-plane of the receiving antenna with lens B.

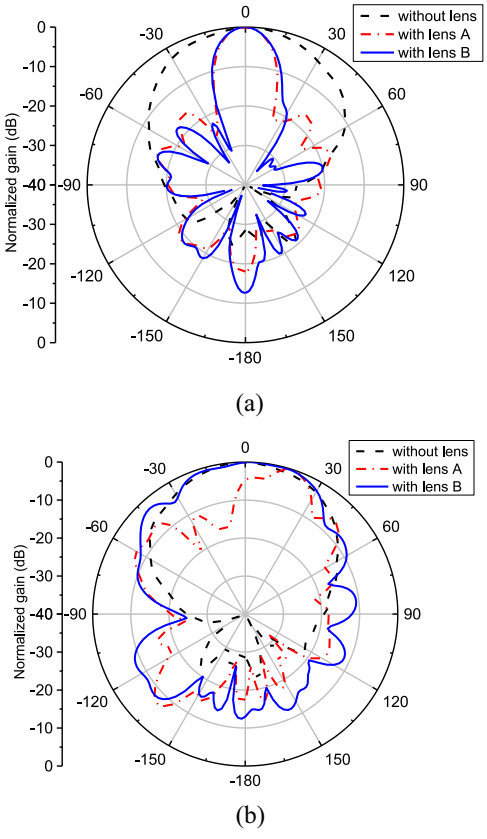

Fig. 9. Comparison of the simulated H-plane pattern for the antenna in three states. (a) Transmitting antenna. (b) Receiving antenna.

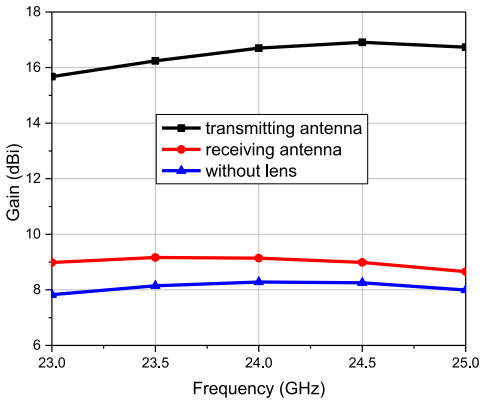

Fig. 10. Comparison of the simulated antenna gain with and without the dual lens.

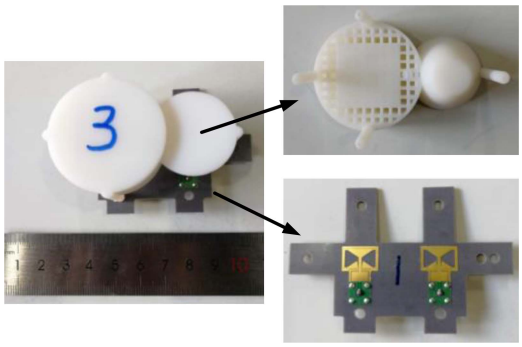

Fig. 11. Photograph of the prototype.

radiation performance of the antenna is measured in a D&M 1900 MMW anechoic chamber designed and manufactured by General Test Systems.

The simulated and measured $|S11|$ results are shown in Fig. 12. The measured $|S11|$ values of the transmitting and receiving antennas are generally below -10 dB from

Authorized licensed use limited to: HUNAN UNIVERSITY. Downloaded on March 04,2021 at 08:46:03 UTC from IEEE Xplore. Restrictions apply.

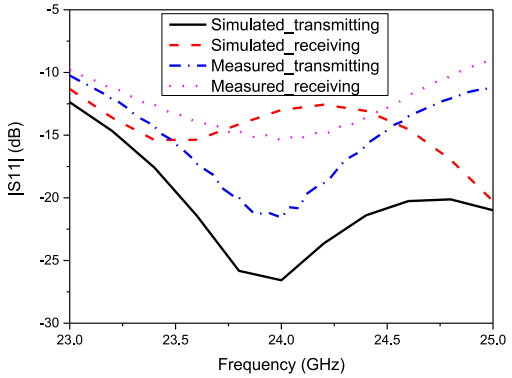

Fig. 12. Simulated and measured |*S*11|.

22 to 25 GHz. The measured |*S*11| trend of the transmitting antenna is consistent with the simulation results, and the position of the resonance point is basically unchanged. The measured result of the receiving antenna has a slight frequency offset as compared with the simulation result. It is likely because the dielectric rod lens is relatively close to the receiving antenna. The inaccuracy of the lens dielectric constant and installation errors may cause this frequency offset.

The simulated and measured radiation patterns at 24 GHz are shown in Fig. 13, which demonstrates that the measured main lobe of the transmitting antenna is in good agreement with the simulation result. The measured side lobes are larger, which may be caused by two reasons: 1) there are simulation errors caused by the inaccuracy of the dielectric constant of the material in the MMW band and 2) because the square holes of the lens are small, there are some errors that arise during processing, which cause the pattern to change. The measured beamwidth of the receiving antenna is approximately 65°, which is approximately 5° wider than the simulated beamwidth. This discrepancy is likely due to the inaccuracy in the permittivity of the lens and substrate and errors in the soldering process.

The simulated and measured gain results are compared shown in Fig. 14. At 24 GHz, the measured transmitting antenna gain is 15.8 dBi, which is approximately 1 dB lower than the simulation result, and the measured receiving antenna gain is 7.9 dBi, which is approximately 1.2 dB lower than that from the simulation. These deviations may arise from installation and soldering errors, test errors, and dielectric loss of the substrate and lens.

B. System Measurement Results

To verify the realistic performance of the designed antenna, the radar system was tested. In Fig. 15, A–G display the test positions of the selected car chassis, and H presents the radar system used in the test. We placed the system under different locations during testing. The selection of test points includes different reflection boundaries on the car chassis, such as flat surfaces, cylindrical surfaces, concave shapes, wedges, and so on.

The test results are shown in Fig. 16. Here, measurement positions 1–7 correspond to positions 1–7 in Fig. 15, and the measurement position 0 represents the case in which there is no vehicle. The ordinate in Fig. 16 gives the amplitude of the sampled reflected signal power after a fast Fourier transform.

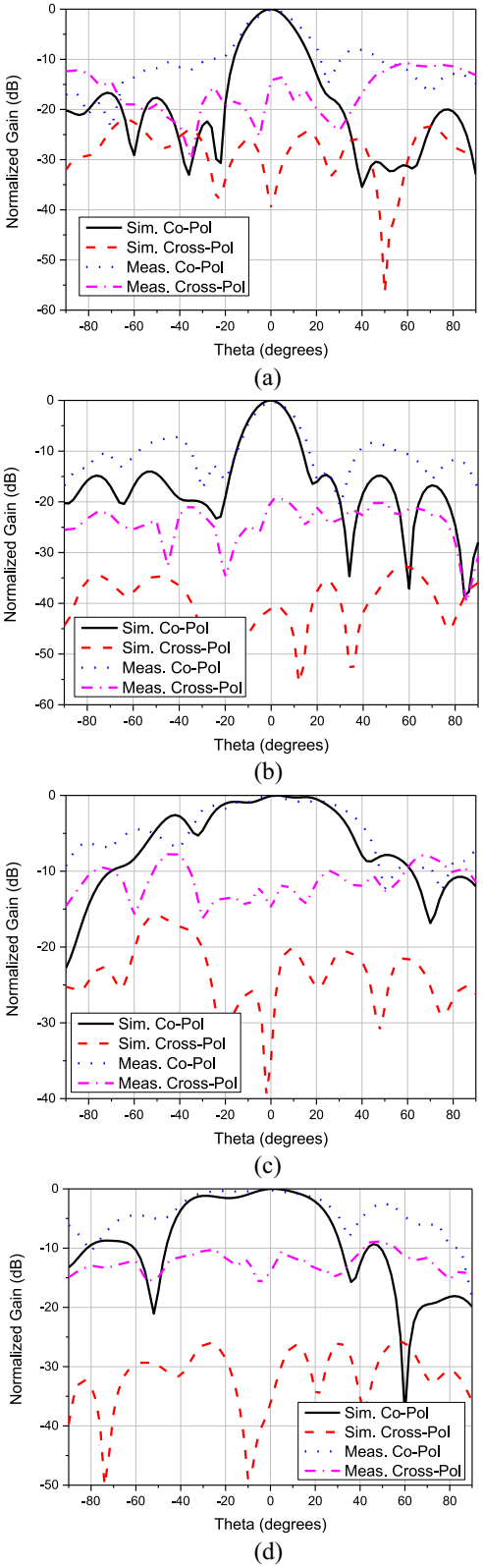

Fig. 13. Simulated and measured patterns at 24 GHz. (a) *H*-plane of the transmitting antenna. (b) *E*-plane of the transmitting antenna. (c) *H*-plane of the receiving antenna. (d) *E*-plane of the receiving antenna.

Authorized licensed use limited to: HUNAN UNIVERSITY. Downloaded on March 04,2021 at 08:46:03 UTC from IEEE Xplore. Restrictions apply.

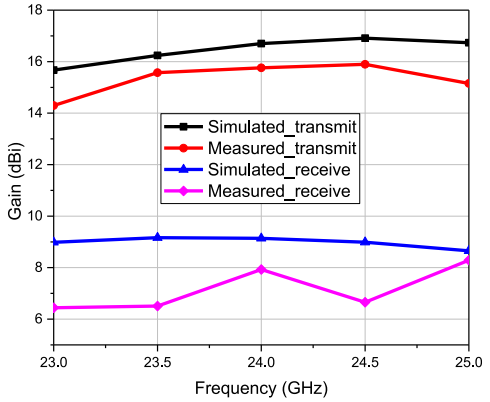

Fig. 14. Simulated and measured gain.

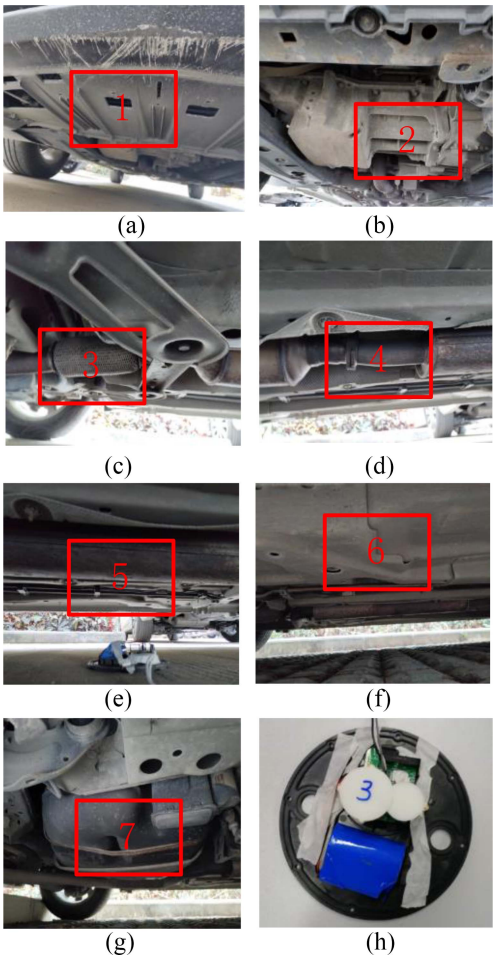

Fig. 15. Photograph of the system measurement setup.

In this study, we use only the maximum value in the available frequency band for comparison. The actual detection algorithm will compare the spectra to detect a vehicle, which is more complicated. The results show that the values measured for the radar system at different positions are much larger than those in the absence of a car (more than 35 000), enabling the system to clearly distinguish the presence or absence of a car or no car under different conditions. Thus, the experimental results demonstrate that the designed antenna performs well.

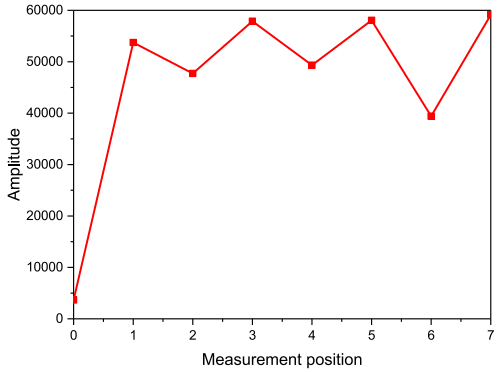

Fig. 16. Measured amplitude for different positions.

Finally, we conducted 1000 experiments by changing the status of the parking spaces. There were only three mistakes in the dual-mode detection system, and the reporting accuracy rate was 99.7%, which is significantly higher than the single geomagnetic system (lower than 90%).

V. Conclusion

A transmitting and receiving dual-lens MMW radar antenna was proposed in this article. A high-gain of the transmitting antenna was achieved by incorporating a flat dielectric perforated lens. Compared with the use of an array to increase the antenna gain, the lens antenna does not require a complicated feeding network and a large area of expensive substrate and expensive processing technology. The proposed approach is a low-loss and low-cost method. A dielectric rod lens is applied to adjust the main beam direction of the receiving antenna. The combined dual-lens ensures that the beam of the receiving antenna is not offset but relatively wide while achieving a high gain of the transmitting antenna. When the antenna is operated at 24 GHz, the measured transmitting antenna gain is 15.8 dBi, the measured receiving antenna gain is 7.9 dBi, and the 3-dB beamwidth is approximately 65°. The system measurement results demonstrate that the antenna can achieve stable measurement results under different situations and is thus suitable for an MMW radar smart parking system.

References

[1] W. Shao, F. D. Salim, T. Gu, N. Dinh, and J. Chan, "Traveling officer problem: Managing car parking violations efficiently using sensor data," *IEEE Internet Things J.*, vol. 5, no. 2, pp. 802–810, Apr. 2018.

[2] C. Li, S. Wang, X. Huang, X. Li, R. Yu, and F. Zhao, "Parked vehicular computing for energy-efficient Internet of Vehicles: A contract theoretic approach," *IEEE Internet Things J.*, vol. 6, no. 4, pp. 6079–6088, Aug. 2019.

[3] Y. Lin, H. Tseng, Y. Lin, and L. Chen, "NB-IoTtalk: A service platform for fast development of NB-IoT applications," *IEEE Internet Things J.*, vol. 6, no. 1, pp. 928–939, Feb. 2019.

[4] X. Sun and N. Ansari, "Dynamic resource caching in the IoT application layer for smart cities," *IEEE Internet Things J.*, vol. 5, no. 2, pp. 606–613, Apr. 2018.

[5] B. Y. Cai, R. Alvarez, M. Sit, F. Duarte, and C. Ratti, "Deep Learning-based video system for accurate and real-time parking measurement," *IEEE Internet Things J.*, vol. 6, no. 5, pp. 7693–7701, Oct. 2019.

[6] L. Hu and Q. Ni, "IoT-driven automated object detection algorithm for urban surveillance systems in smart cities," *IEEE Internet Things J.*, vol. 5, no. 2, pp. 747–754, Apr. 2018.

Authorized licensed use limited to: HUNAN UNIVERSITY. Downloaded on March 04,2021 at 08:46:03 UTC from IEEE Xplore. Restrictions apply.

[7] H. Dong, X. Wang, C. Zhang, R. He, L. Jia, and Y. Qin, "Improved robust vehicle detection and identification based on single magnetic sensor," *IEEE Access*, vol. 6, pp. 5247–5255, 2018.
[8] X. Chen, X. Kong, M. Xu, K. Sandrasegaran, and J. Zheng, "Road vehicle detection and classification using magnetic field measurement," *IEEE Access*, vol. 7, pp. 52622–52633, 2019.
[9] Q. Wang, J. Zheng, H. Xu, B. Xu, and R. Chen, "Roadside magnetic sensor system for vehicle detection in urban environments," *IEEE Trans. Intell. Transp. Syst.*, vol. 19, no. 5, pp. 1365–1374, May 2018.
[10] L. Lou, J. Zhang, Y. Xiong, and Y. Jin, "Robust static vehicle detection method based on the fusion of GPS SNR and magnetic signal," *IEEE Sensors J.*, vol. 19, no. 21, pp. 10111–10120, Nov. 2019.
[11] Z. Zhang, X. He, and H. Yuan, "A robust parking detection algorithm against electric railway magnetic field interference," *IEEE Trans. Intell. Transp. Syst.*, vol. 21, no. 2, pp. 882–893, Feb. 2020.
[12] H. Qi, "Design of wireless parking space detector based on geomagnetic and radar detection," *Meas. Control Technol.*, vol. 37, no. 7, pp. 78–81, Jul. 2018.
[13] V. Basavarajappa, A. Pellon, I. Montesinos-Ortego, B. B. Exposito, L. Cabria, and J. Basterrechea, "Millimeter-wave multi-beam waveguide lens antenna," *IEEE Trans. Antennas Propag.*, vol. 67, no. 8, pp. 5646–5651, Aug. 2019.
[14] M. Chen, A. Epstein, and G. V. Eleftheriades, "Design and experimental verification of a passive Huygens' metasurface lens for gain enhancement of frequency-scanning slotted-waveguide antennas," *IEEE Trans. Antennas Propag.*, vol. 67, no. 7, pp. 4678–4692, Jul. 2019.
[15] N. Zhang, W. X. Jiang, H. F. Ma, W. X. Tang, and T. J. Cui, "Compact high-performance lens antenna based on impedance-matching gradient-index metamaterials," *IEEE Trans. Antennas Propag.*, vol. 67, no. 2, pp. 1323–1328, Feb. 2019.
[16] K. X. Wang and H. Wong, "Design of a wideband circularly polarized millimeter-wave antenna with an extended hemispherical lens," *IEEE Trans. Antennas Propag.*, vol. 66, no. 8, pp. 4303–4308, Aug. 2018.
[17] H. Xu, J. Zhou, K. Zhou, Q. Wu, Z. Yu, and W. Hong, "Planar wideband circularly polarized cavity-backed stacked patch antenna array for millimeter-wave applications," *IEEE Trans. Antennas Propag.*, vol. 66, no. 10, pp. 5170–5179, Oct. 2018.
[18] A. Dewantari, J. Kim, I. Scherbatko, and M. Ka, "A sidelobe level reduction method for mm-Wave substrate integrated waveguide slot array antenna," *IEEE Antennas Wireless Propag. Lett.*, vol. 18, pp. 1557–1561, 2019.
[19] J. Cao, H. Wang, S. Mou, P. Soothar, and J. Zhou, "An air cavity-fed circularly polarized magneto-electric dipole antenna array with gap waveguide technology for mm-Wave applications," *IEEE Trans. Antennas Propag.*, vol. 67, no. 9, pp. 6211–6216, Sep. 2019.
[20] M. Sun, X. Qing, and Z. N. Chen, "60-GHz end-fire fan-like antennas with wide beamwidth," *IEEE Trans. Antennas Propag.*, vol. 61, no. 4, pp. 1616–1622, Apr. 2013.
[21] Y. Li and K. Luk, "A linearly polarized magnetoelectric dipole with wide H-plane beamwidth," *IEEE Trans. Antennas Propag.*, vol. 62, no. 4, pp. 1830–1836, Apr. 2014.
[22] M. D. Migliore and D. Pinchera, "Correction of beam direction in adaptive parasitic monopole arrays using a truncated cone structure," *IEEE Antennas Wireless Propag. Lett.*, vol. 11, pp. 1486–1488, 2012.
[23] L. Ge and K. M. Luk, "Beamwidth reconfigurable magneto-electric dipole antenna based on tunable strip grating reflector," *IEEE Access*, vol. 4, pp. 7039–7045, 2016.
[24] L. Ge and K. Luk, "Linearly polarized and dual-polarized magneto-electric dipole antennas with reconfigurable beamwidth in the H-plane," *IEEE Trans. Antennas Propag.*, vol. 64, no. 2, pp. 423–431, Feb. 2016.
[25] S. Qu, J. Li, and Q. Xue, "Bowtie dipole antenna with wide beamwidth for base station application," *IEEE Antennas Wireless Propag. Lett.*, vol. 6, pp. 293–295, 2007.
[26] G. E. Mueller and W. A. Tyrrell, "Polyrod antennas," *Bell Sys. Techn. J.*, vol. 26, no. 4, pp. 837–851, Oct. 1947.
[27] P. Andres-Maldonado, M. Lauridsen, P. Ameigeiras, and J. M. Lopez-Soler, "Analytical modeling and experimental validation of NB-IoT device energy consumption," *IEEE Internet Things J.*, vol. 6, no. 3, pp. 5691–5701, Jun. 2019.
[28] V. Petrov *et al.*, "Vehicle-based relay assistance for opportunistic crowdsensing over narrowband IoT (NB-IoT)," *IEEE Internet Things J.*, vol. 5, no. 5, pp. 3710–3723, Oct. 2018.
[29] G. Tsoukaneri, M. Condoluci, T. Mahmoodi, M. Dohler, and M. K. Marina, "Group communications in narrowband-IoT: Architecture, procedures, and evaluation," *IEEE Internet Things J.*, vol. 5, no. 3, pp. 1539–1549, Jun. 2018.
[30] P. Fei, Y. Qi, and Y. Jiao, "Design of a wideband dual-element slot loop antenna array with adjustable back-reflector," *IEEE Antennas Wireless Propag. Lett.*, vol. 11, pp. 1014–1017, 2012.
[31] X. Gao, Y. Qi, and Y. C. Jiao, "Design of multiplate back-reflector for a wideband slot antenna," *IEEE Antennas Wireless Propag. Lett.*, vol. 12, pp. 773–776, Jun. 2013.
[32] Z. Cai, Y. Qi, Z. Weng, W. Yu, F. Li, and J. Fan, "DC ground compact wideband omnidirectional vertically polarised slot loop antenna for 4G long-term evolution applications," *IET Microw. Antennas Propag.*, vol. 12, no. 7, pp. 1087–1092, Jun. 2018.
[33] Y. Xiao, Y. Qi, F. Li, J. Fan, W. Yu, and L. Lu, "Dual-band directional slot antenna for Wi-Fi application," *IEEE Trans. Antennas Propag.*, vol. 66, no. 8, pp. 4277–4281, Aug. 2018.
[34] L. Chi, Y. Qi, Z. Weng, W. Yu, F. Li, and J. L. Drewniak, "Directional antenna with consistent H-plane dual-band beamwidth for Wi-Fi applications," *IEEE Trans. Antennas Propag.*, vol. 67, no. 7, pp. 4495–4505, Jul. 2019.
[35] L. Chi, Y. Qi, Z. Weng, W. Yu, and W. Zhuang, "A compact wideband slot-loop directional antenna for marine communication applications," *IEEE Trans. Veh. Technol.*, vol. 68, no. 3, pp. 2401–2412, Mar. 2019.

Zhanghua Cai (Student Member, IEEE) received the B.S. and M.S. degrees in electronic information and technology from Hunan University, Changsha, China, in 2014 and 2017, respectively, where he is currently pursuing the Ph.D. degree in electronics.

His current research interests include end-fire directional antennas, millimeter-wave antennas, and antenna arrays.

Yantao Zhou received the Ph.D. degree in information and electrical engineering from Wuhan Naval University of Engineering, Wuhan, China, in 2009.

He is currently a Professor of electric and information engineering with Hunan University, Changsha, China. His major research contains parallel computing and distributed data management.

Yihong Qi (Senior Member, IEEE) received the Ph.D. degree in electronics from Xidian University, Xi'an, China, in 1989.

He was a Postdoctoral Fellow and an Associate Professor with the Southeast University, Nanjing, China. From 1993 to 1995, he was a Postdoctoral Researcher with McMaster University, Hamilton, ON, Canada. From 1995 to 2010, he was with Research in Motion (Blackberry), Waterloo, ON, Canada, where he was the Director of advanced electromagnetic research. He is currently the President and a Chief Scientist with General Test Systems, Inc., Shenzhen, China. He is also an Adjunct Professor with the EMC Laboratory, Missouri University of Science and Technology, Rolla, MO, USA; Hunan University, Changsha, China; and Western University, London, ON, Canada; and an Honorary Professor with Southwest Jiaotong University, Chengdu. He is an inventor of more than 450 published and pending patents.

Dr. Qi has received the IEEE EMC Society Technical Achievement Award in August 2017. He was a Distinguished Lecturer of IEEE EMC Society in 2014 and 2015 and served as the Chairman of IEEE EMC TC-12. He is a Fellow of the Canadian Academy of Engineering and the National Academy of Inventors.

Authorized licensed use limited to: HUNAN UNIVERSITY. Downloaded on March 04,2021 at 08:46:03 UTC from IEEE Xplore. Restrictions apply.

Weihua Zhuang (Fellow, IEEE) received the B.Sc. and M.Sc. degrees in electrical engineering from Dalian Maritime University, Dalian, China, and the Ph.D. degree in electrical engineering from the University of New Brunswick, Fredericton, NB, Canada, in October 1993.

She has been with the Department of Electrical and Computer Engineering, University of Waterloo, Waterloo, ON, Canada, since 1993, where she is a Professor and a Tier I Canada Research Chair of wireless communication networks.

Dr. Zhuang is a recipient of the Technical Recognition Award from IEEE Communications Society Ad Hoc & Sensor Networks Technical Committee in 2017, and a co-recipient of several best paper awards from IEEE conferences. She was the Editor-in-Chief of the IEEE TRANSACTIONS ON VEHICULAR TECHNOLOGY from 2007 to 2013, the Technical Program Chair/Co-Chair of IEEE VTC 2017 Fall and 2016 Fall, and the Technical Program Symposia Chair of the IEEE Globecom 2011. She is a Fellow of the Royal Society of Canada, the Canadian Academy of Engineering, and the Engineering Institute of Canada. She is an elected member in the Board of Governors and VP Publications of the IEEE Vehicular Technology Society. She was an IEEE Communications Society Distinguished Lecturer from 2008 to 2011.

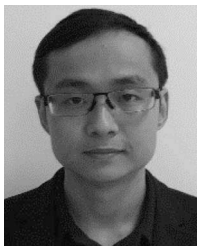

Lei Deng (Member, IEEE) received the B.E. and M.E. degrees in electrical engineering from Huazhong University of Science and Technology, Wuhan, China, in 2008 and 2012, respectively. He is currently pursuing the Ph.D. degree with Hunan University, Changsha, China.

His research interests include IoT-based data management and applications.

Authorized licensed use limited to: HUNAN UNIVERSITY. Downloaded on March 04,2021 at 08:46:03 UTC from IEEE Xplore. Restrictions apply.